Whole-Body ^{18}F-FDG PET/CT in the Presence of Truncation Artifacts

Thomas Beyer, PhD[1]; Andreas Bockisch, MD, PhD[1]; Hilmar Kühl, MD[2]; and Maria-Jose Martinez, PhD[3]

[1]Department of Nuclear Medicine; University Hospital Essen, Essen, Germany; [2]Institute of Diagnostic and Interventional Radiology and Neuroradiology; University Hospital Essen, Essen, Germany; and [3]Department of Nuclear Medicine; Technical University Munich, Munich. Germany

We investigated the effect of CT truncation in whole-body (WB) PET/CT imaging of large patients, and we evaluated the efficacy of an extended field-of-view (eFOV) correction technique. **Methods:** Two uniform phantoms simulating a ''torso'' and an ''arms-up'' setup were filled with ^{18}F-FDG/water. A third, nonuniform ''body phantom was prepared with hot and cold lesions. All 3 phantoms were positioned in the center of the PET/CT gantry with ≥10% of their volume extending beyond the maximum CT FOV. An eFOV algorithm was used to estimate complete CT projections from nonlinear extrapolation of the truncated projections. CT-based attenuation correction (CT AC) of the phantom data was performed using CT images reconstructed from truncated and extended projections. For clinical validation, we processed truncated datasets from 10 PET/CT patients with and without eFOV correction. **Results:** When using truncated CT images for CT AC, PET tracer distribution was suppressed outside the transverse CT FOV in phantom and patient studies. PET activity concentration in the truncated regions was only 10%–32% of the true value but increased to 84%–100% when using the extended CT images for CT AC. At the same time, the contour of phantoms and patients was recovered to the anatomically correct shape from the uncorrected emission images, and the apparent distortion of lesions near the maximum CT FOV was reduced. **Conclusion:** Truncation artifacts in WB PET/CT led to visual and quantitative distortions of the CT and attenuation-corrected PET images in the area of truncation. These artifacts can be corrected to improve the accuracy of PET/CT for diagnosis and therapy response evaluation.

Key Words: combined PET/CT; truncation effects; image quality; image artifacts

J Nucl Med 2006; 47:91–99

Combined imaging with PET/CT has become a routine modality for diagnostic oncology (*1*). PET/CT tomographs represent a hardware approach to image fusion by merging the components of commercially available PET and CT tomographs into a single gantry (*2*). Patients are scheduled for a single scan and receive 2 complementary examinations (PET and CT) whenever clinically indicated.

In addition to the intrinsically coregistered metabolic and anatomic information from PET and CT, respectively, the CT data are used for attenuation correction (AC) of the PET emission data (*3,4*). By using the essentially noiseless CT transmission images instead of the standard PET transmission images, noise propagation through CT-based AC is limited and cross-contamination from the emission data is avoided.

However, in almost all available PET/CT systems today, the measured transverse field of view (FOV) of CT is 50 cm, whereas that of PET is 60 cm (*5*). This difference in the maximum measured FOV between CT and PET may lead to truncation artifacts if patients are positioned less carefully on the PET/CT patient handling system in such a way that part of their body extends beyond the CT FOV or if particularly large patients are scanned. As a result, truncation may lead to overshoot artifacts in the CT images at the limit of the FOV in the vicinity of the truncated object.

In this study we investigated CT truncation artifacts in whole-body (WB) PET/CT and we evaluated the efficacy of a simple extended FOV (eFOV) correction technique for improved AC in PET/CT.

MATERIALS AND METHODS

Phantom Studies

Truncation artifacts in WB PET/CT situations were studied in a series of 3 phantom setups. In all studies the phantom was first centered in the transverse FOV of the PET/CT and scanned (center position) before the phantom was positioned and scanned in an off-center setup to simulate truncation (offset_trunc position).

PHANTOM A (Baseline). A 20-cm plastic cylinder filled with water and ^{18}F-FDG (9.6 kBq/mL) was centered in the transverse FOV of the PET/CT. In a second setup, the same cylinder was moved 19 cm off-center to simulate truncation of the CT images (Fig. 1A).

PHANTOM B ("ARMS-UP"). Two 1.5-L plastic bottles were placed next to a 20-cm plastic cylinder. All 3 containers were filled with water and ^{18}F-FDG (2.9 kBq/mL). Compared with a WB patient study, the main cylinder and the 2 bottles simulate the head and the arms raised above the head, respectively. First,

Received Jul. 21, 2005; revision accepted Sep. 29, 2005.

For correspondence contact: Thomas Beyer, PhD, Department of Nuclear Medicine, University Hospital Essen, Hufelandstrasse 55, D 45122 Essen, Germany.

E-mail: thomas.beyer@uni-essen.de

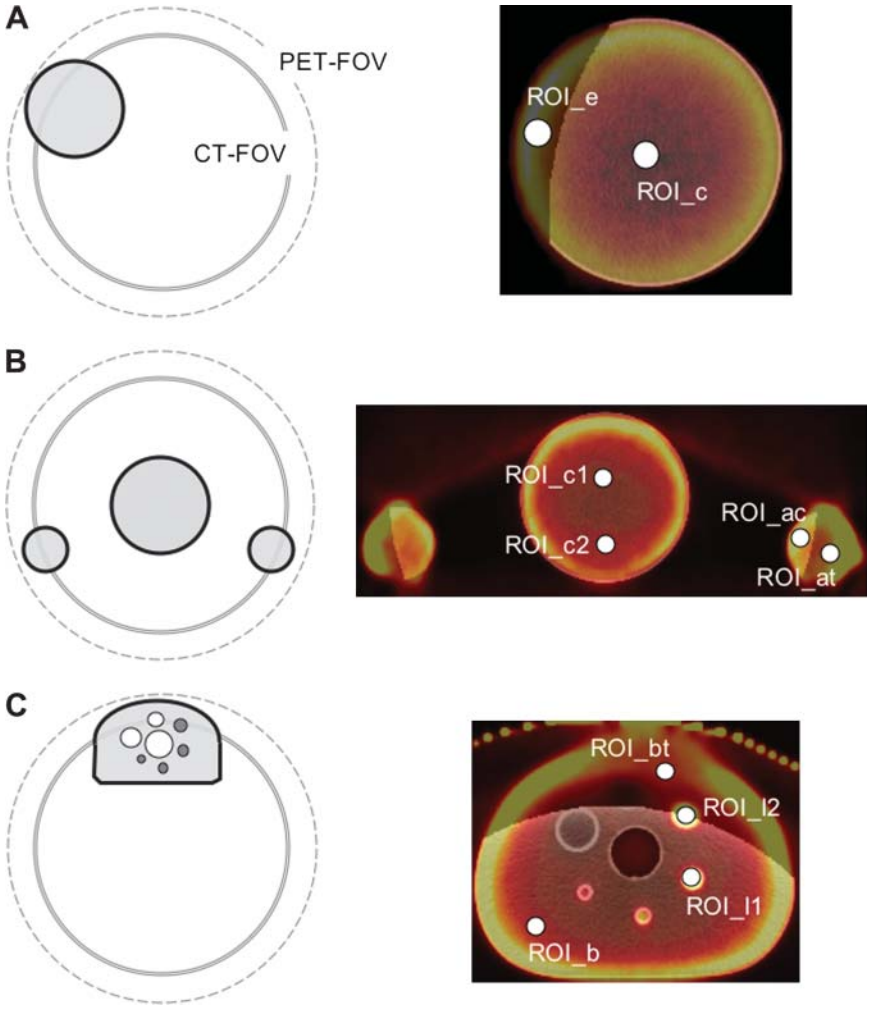

FIGURE 1. Phantom setups for object truncation (offset_trunc). Experimental outline is shown to the left and fused PET/CT before AC is shown to the right. (A) A 20-cm cylinder filled with ^{18}F-FDG and water was placed at edge of CT FOV (double line). (B) The same cylinder simulating the trunk was centered and with 2 arms (8-cm diameter each) placed at edge of CT FOV. (C) National Electrical Manufacturers Association (NEMA)-quality phantom with 4 hot lesions (9:1 background ratio) was placed off-center. All phantom arrangements were contained within measured PET FOV (dashed line). ROIs were defined on corresponding fused uncorrected PET/CT images (right column). ROI_e = truncated/extended area; ROI_c = center; ROI_c1 and ROI_c2 = center of central cylinder; ROI_ac = central arm; ROI_at = truncated arm; ROI_b = background body; ROI_l1 = lesion 1; ROI_l2 = lesion 2; ROI_bt = background truncated. For each phantom study, regions of interest (ROIs) were the same size.

the phantom was centered in the CT FOV before moving both arms sideways to simulate truncation of the arms (Fig. 1B).

PHANTOM C ("LARGE TRUNK"). To simulate imaging the trunk without and with truncation, a National Electrical Manufacturers Association (NEMA) NU2-2001 image-quality phantom (*6*) was filled with water and ^{18}F-FDG. The phantom is $40 \times 30 \times 20$ cm^3 in size and contains 6 hollow spheres of different inner diameters (11–37 mm), simulating lesions. Of these 6 spheres, 4 were filled with water and ^{18}F-FDG with a lesion-to-background ratio of 9:1 at a background activity concentration of 5.8 kBq/mL. The 2 largest spheres were filled with inactive water, only to simulate cold lesions The body phantom was scanned in the center of the CT FOV and 20 cm off-center (Fig. 1C).

PET/CT Acquisition

All scans were performed on a combined PET/CT tomograph (Biograph Sensation 16; Siemens Molecular Imaging). The PET components of the PET/CT resemble those of a stand-alone ECAT ACCEL with a 6.7-mm spatial resolution, except the side shielding was reduced to match the 70-cm inner gantry diameter of the CT. The CT components of the PET/CT correspond to a 16-slice spiral CT (Sensation 16; Siemens Medical Solutions) with a transverse FOV of 50 cm and an in-plane spatial resolution of <1 mm. The combined system is complemented by a revised patient handling system with a fixed fulcrum cantilever bed moving on rails in and out of the gantry, thus avoiding any relative vertical displacement between the CT and the PET.

Each PET/CT scan of phantoms A–C in the center and offset_trunc position was preceded by an overview scan (topogram) to ensure accurate phantom positioning with respect to the transverse FOV. A spiral, low-dose CT scan was acquired over the axial range of 16.2 cm, corresponding to a single bed position of the PET. Default CT scan parameters were 120 kVp and 15 mA. After the CT scan, the phantom was moved automatically to the PET toward the rear of the gantry where emission scanning over the coaxial imaging range (1 bed position) commenced. Emission scan time was 10 min.

Emission images were reconstructed iteratively (Fourier rebinning [FORE] + attenuation-weighted ordered-subset expectation maximization [AWOSEM], 4 iterations and 8 subsets, 5-mm gaussian filter) without and with CT-based AC as described first by Kinahan et al. (*3,7*). In case of CT truncation, when phantoms were positioned and scanned at the offset_trunc position, CT-based AC was also performed on the basis of the extended CT FOV transmission data (offset_ext) (*8*).

Extended CT FOV

Among a choice of correction methods to recover truncated projection data, we used a simple algorithm proposed by Ohnesorge et al. (*9*) and implemented on several commercially

available CT systems. In brief, this algorithm is based on 4 steps (Fig. 2).

First, the truncated CT projections are extrapolated to the predefined limit of the extended FOV, which matches that of the measured PET FOV (60 cm). Thereby, the truncated projections are continued symmetrically by mirroring the projection at the maximum CT FOV (Fig. 2A). A cosine roll-off filter is applied to the extrapolated projections to force the projection values to zero at the limit of the eFOV (Fig. 2B). Before using the extended projections to reconstruct the images (step 4), a smoothing kernel is used to limit noise contributions from the mirrored portions of the measured projections (Fig. 2C). The generated extended CT images were exported in standard CT DICOM (Digital Imaging and Communications in Medicine) format and used for CT AC of the complementary emission data (*8*).

Phantom Data Analysis

To describe the magnitude of truncation in all 3 phantom experiments we first estimated the amount of volume truncation on CT by subtracting the reconstructed CT volume of the imaged phantom at the off-center position (offset_trunc) without eFOV correction from the known volume of the phantom. Truncation effects were assessed visually by comparing image overlays of the CT with PET before and after AC based on the truncated CT data. Small circular regions of interest (ROIs) in the truncated areas and nontruncated, central regions were defined on the fused uncorrected PET emission and CT images (Fig. 1). The ROIs were defined on the central axial plane of the phantom and copied into the 5 nearest image planes above and below the central plane. Average ROI values and SD were calculated from these 11 central image planes. For the 2 spheric lesions in phantom C we used only singular planar ROI values in the axial plane with the maximum appearance of the 2 lesions. Average and singular ROI values were used for subsequent quantitative analysis of the CT attenuation values and attenuation-corrected PET activity in phantoms A and B and in phantom C, respectively.

Student *t* tests (2-tailed, paired) with Bonferroni correction were performed separately for the CT and PET data to assess the statistical significance of differences between the ROI values. The central ROI values in the center position of the phantom were used as the reference values. All ROI estimates in the truncated region (before and after eFOV correction, offset_trunc, and offset_ext) were tested against this reference.

Patient Studies

The correction algorithm for CT truncation was applied to 10 clinical WB PET/CT studies from our clinical routine operation. Truncation artifacts on CT were pointed out by the expert readers, and patient studies were reprocessed retrospectively off-line. Of these 10 patient studies, 5 each were acquired on PET/CT using 2-slice and 16-slice CT, respectively (group PET/CT2 and PET/CT16). Both CT systems have a 50-cm transverse FOV, and truncated CT projections were corrected by the same algorithm described above (*9*). Incidentally, CT truncation was observed only in the area of the arms in the case of the 2-slice PET/CT. In the case of the 16-slice PET/CT, CT truncation was observed in the area of the arms and the lower trunk.

All patients were studied following the same imaging protocols, whereby a topogram scan was followed by a single spiral CT and a multibed emission scan covering the same area as the CT. Patients in both groups were given breath-hold commands (*10*) to limit the amount of motion-induced misregistration in the upper diaphragm. In addition, intravenous and oral CT contrast material was used in study group PET/CT2 (*11,12*) but not in PET/CT16.

Emission images were reconstructed after CT AC based on the original truncated and the extended CT transmission images. Corrected emission images were compared visually because, in the absence of a known local activity distribution, no absolute quantitative assessment of the tracer activity was possible. The outline of the attenuation-corrected tracer distribution was also compared with the uncorrected emission data.

RESULTS

Phantom Studies

PHANTOM A. The amount of volume truncation in the offset_trunc position was 17%. Figure 3 shows axial CT and PET image planes of the phantom being positioned in the center and at the edge of the FOV (offset_trunc), without and with truncation artifacts, respectively. Volume truncation lead to a masking effect of the reconstructed PET activity (Fig. 3B), which was not fully recovered within the extent of the uncorrected tracer distribution (noAC PET). The results of the ROI analysis are summarized in Table 1. Tracer activity in the truncated region (ROI_e) was only 17% of the nominal activity in the center of the phantom (ROI_c). When applying the eFOV

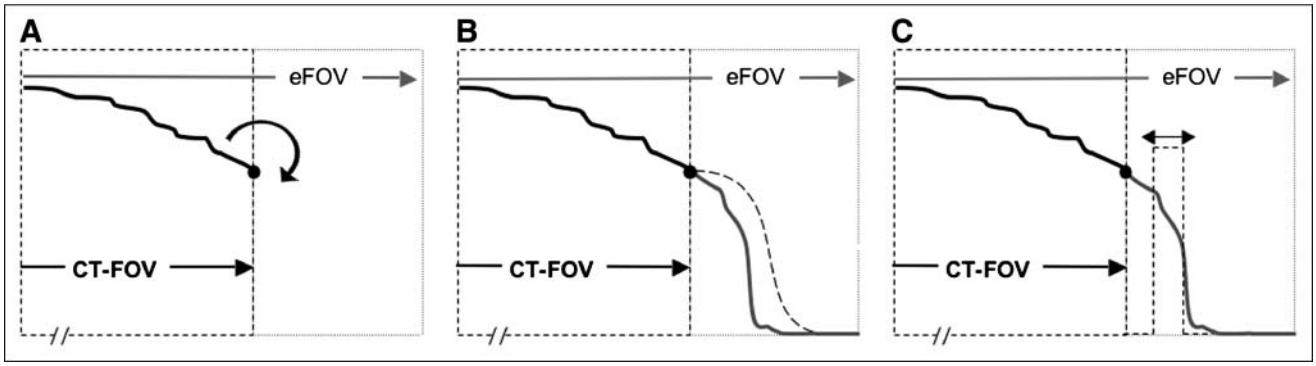

FIGURE 2. Outline of eFOV algorithm used in this study (*9*). Mirror truncated projections at maximum CT FOV to extrapolate the projections to limit of PET FOV (eFOV) (A), apply a cosine roll-off filter to extrapolated projections (B), apply a 25-channel smoothing kernel to filtered extended projections, and backproject extrapolated and filtered projections (not shown).

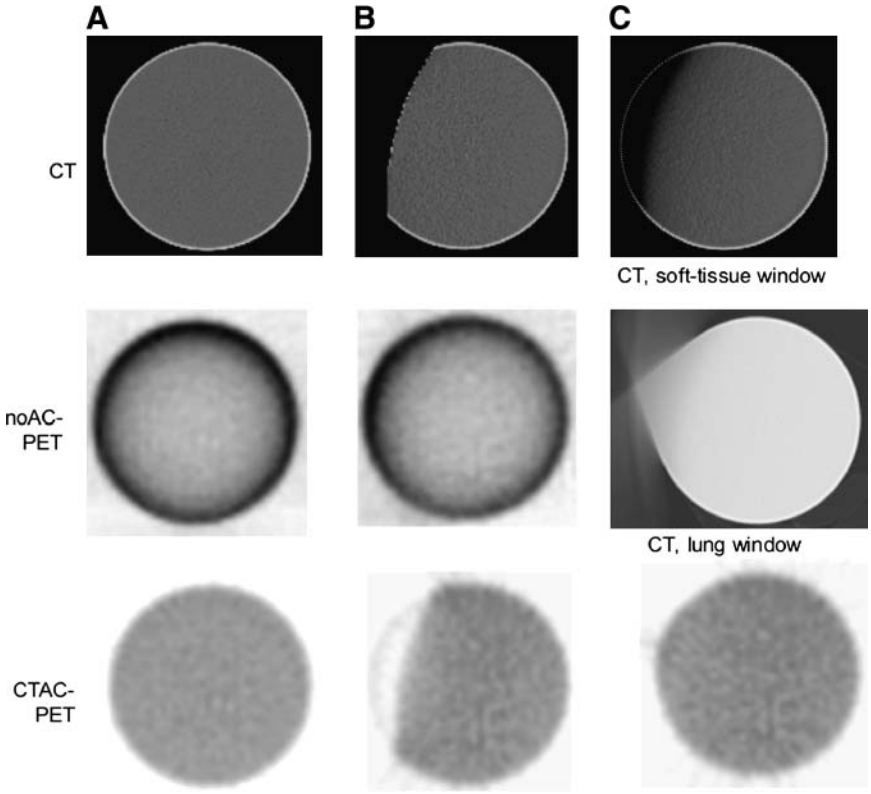

FIGURE 3. Phantom A. Axial CT images and PET images before (noAC) and after CT-based AC (CTAC) for phantom positioned centrally inside the FOV (A), phantom moved to edge of the FOV with 17% volume truncation (offset_trunc position) (B), and as (B) but after eFOV correction (offset_ext) (C). CT images are shown in soft-tissue window (top) and lung window (middle).

correction to the CT data, CT attenuation was recovered to –150 Hounsfield units (HU) (compared with the true value of 0 HU for water), and the corrected PET activity in the truncated region was recovered to within 90% of the injected activity concentration (8.7 kBq/mL over 9.7 kBq/mL).

PHANTOM B. With the left and right arm positioned on the edge of the CT FOV, the amount of volume truncation was 5% overall and 75% of the left arm alone. Figure 4 shows central CT and PET image planes of the phantom without and with truncation artifacts. We evaluated the effect of truncation in the left arm only because it displays the maximum effect of truncation (Table 2).

First, the introduction of the arms caused beam-hardening effects, which generated lateral streaks across the arms (Fig. 4A) and which affected the CT attenuation values as seen from a comparison of ROI_c2 and ROI_at with the unaffected ROI_c1 (Table 2).

As shown in Figure 4, truncation artifacts in the left and right side of the phantom masked the reconstructed PET activity, which was not recovered within the extent of the uncorrected tracer distribution (noAC PET). The reconstructed PET activity in the left arm inside (ROI_ac) and outside (ROI_at) the CT FOV was reduced to 70% and 30% of the standard central activity, respectively. When applying

TABLE 1
Phantom A: Average CT Attenuation (HU) and PET Activity (kBq/mL) and SD in ROIs at Center (ROI_c) and Edge (ROI_e)

Image	Phantom position	ROI_c (HU)	*t* test (*P* value)	ROI_e (HU)	*t* test (*P* value)
CT	Center	−1 ± 9	NA	−1 ± 7	0.5 (NS)
	offset_trunc	−5 ± 14	<0.001	—	NA
	offset_ext	−10 ± 9	<0.001	−150 ± 70	<0.001
		(kBq/mL)		(kBq/mL)	
PET	Center	9.7 ± 0.5	NA	9.7 ± 0.4	4.6 (NS)
	offset_trunc	9.7 ± 0.5	4.6 (NS)	1.7 ± 0.8	<0.001
	offset_ext	9.4 ± 0.5	<0.001	8.7 ± 0.5	<0.001

NA = not applicable; NS = not statistically significant.

For location of ROIs, see Figure 1A. *P* values for CT and PET indicate statistical significance in a 2-tailed, paired Student *t* test with Bonferroni correction in reference to central ROI (ROI_c).

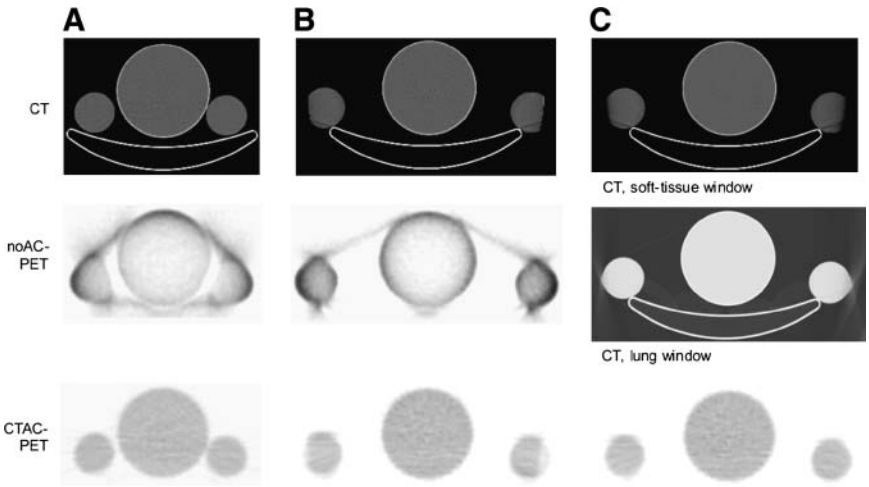

FIGURE 4. Phantom B. Axial CT images and PET images before (noAC) and after CT-based AC (CTAC) for phantom positioned centrally inside the FOV (A), phantom moved to edge of the FOV (offset_trunc position) (B), and as (B) but after eFOV correction (offset_ext) (C). CT images of after eFOV correction are shown in soft-tissue window and lung window for better appreciation of recovered CT object.

the eFOV correction, CT attenuation in the truncated portion of the phantom (water) was recovered (−110 HU) and the corresponding AC PET activity concentration increased to the standard activity level. However, at the same time CT attenuation inside in the vicinity of the maximum CT FOV (ROI_ac) was affected also, and the corresponding PET activity was only 82% of the standard activity (Table 2).

PHANTOM C. The amount of volume truncation in the offset_trunc position was 10%. Figure 5 shows the axial CT and PET images before and after the eFOV correction was applied. Table 3 summarizes the quantitative analysis. In the offset_trunc position, CT attenuation values of the background (ROI_b) changed significantly. Truncation of the upper portion of the phantom (Fig. 5) led to a 90% underestimation of the attenuation-corrected PET activity in the phantom background region (ROI_bt), and only 50% and 20% recovery of the activity of the lesion that was near (ROI_l1) and on the edge (ROI_l2) of the CT FOV, respectively. When using the extended CT images for AC, the PET activity in the truncated background was recovered, and the tracer activity in the selected lesions was recovered to within 85% of the known activity.

Patient Studies

The eFOV correction could be applied to all patient data and the reconstructed PET activity was recovered within the boundaries of the uncorrected emission data. This is illustrated in Figures 6A and 6B for a patient study from a PET/CT system using a 2-slice and a 16-slice CT system, respectively. The coronal images demonstrate that the extent of the tracer distribution in the AC PET after the eFOV correction was effectively the same as that in the uncorrected PET images (noAC), which are not affected by truncation artifacts.

Because of a lack of knowledge of the true attenuation and PET activity values in these patients, the effect of truncation and eFOV correction is best appreciated in

TABLE 2
Phantom B: Average CT Attenuation (HU) and PET Activity (kBq/mL) and SD in 4 ROIs: ROI_c1 and ROI_c2 in Main Cylinder Above and Within Lateral Streak Artifacts Arising from Beam Hardening Along Arms, ROI_ac and ROI_at in Arms Inside and Outside of Maximum FOV

Image	Phantom position	ROI_c1 (HU)	*t* test (*P* value)	ROI_c2 (HU)	*t* test (*P* value)	ROI_ac (HU)	*t* test (*P* value)	ROI_at (HU)	*t* test (*P* value)
CT	Center	−1 ± 14	NA	−1 ± 14	0.4 (NS)	−3 ± 10	<0.001	−3 ± 9	0.04
	offset_trunc	0 ± 13	1 (NS)	1 ± 13	<0.07	14 ± 14	0.001	—	NA
	offset_ext	−7 ± 8	<0.001	−6 ± 8	<0.08	−82 ± 18	<0.001	−110 ± 80	<0.001
		(kBq/mL)		(kBq/mL)		(kBq/mL)		(kBq/mL)	
PET	Center	2.8 ± 0.2	NA	2.9 ± 0.2	0.02	2.8 ± 0.2	4	2.9 ± 0.1	<0.03
	offset_trunc	2.9 ± 0.1	1	3.0 ± 0.2	<0.001	2.0 ± 0.5	<0.001	0.94 ± 0.06	<0.001
	offset_ext	3.0 ± 0.2	<0.001	2.9 ± 0.1	<0.001	2.3 ± 0.3	<0.001	3.0 ± 0.4	<0.02

For location of the ROIs, see Figure 1B. The *P* values were calculated for the CT and PET values independently and in reference to the central ROI (ROI_c1) using the 2-tailed, paired Student *t* test with Bonferroni correction.

NA = not applicable; NS = not statistically significant.

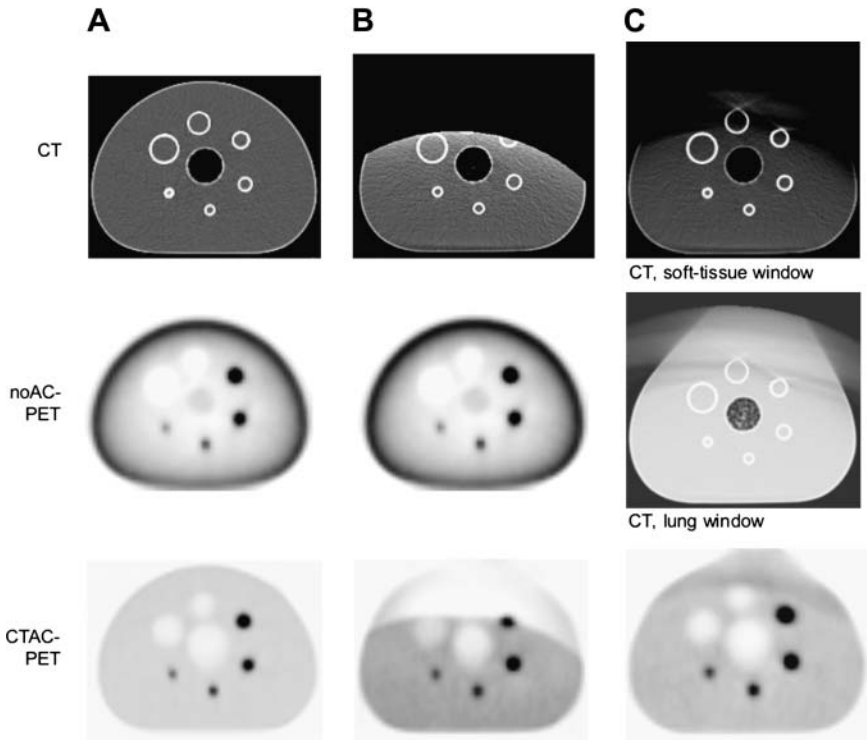

FIGURE 5. Phantom C. Axial CT images and PET images before (noAC) and after CT-based AC (CTAC) for phantom positioned centrally inside the FOV (A), phantom moved to the edge of the FOV such that the largest hot lesion is on edge of the CT FOV (offset_trunc position) (B), and as (B) but after eFOV correction (offset_ext) (C). CT images after eFOV correction are shown also in soft-tissue window and lung window.

lateral profiles through the center of the axial patient images (Figs. 6C and 6D). The full and dotted line graphs in Figure 6C represent the profiles through the CT along the white line indicated in Figure 6A with the limited and extended CT FOV, respectively. Similarly, the profiles through the PET after AC based on the truncated and extended CT FOV are shown in Figure 6D. In both graphs (Figs. 6C and 6D), the profile through the uncorrected PET images (noAC PET) is shown for reference. The resulting object and tracer recovery on CT and PET, respectively, can be appreciated on either side of the profile beyond the CT FOV. The slight amplification of the tracer concentration inside the CT FOV was <30% (pixel-based).

DISCUSSION

This study was performed to estimate the effect of truncation artifacts in combined, WB PET/CT. Truncation artifacts may arise when positioning patients away from the in-plane center of the PET/CT gantry or when imaging large patients. Based on phantom scans we were able to replicate the known masking artifacts from clinical PET/CT. Our

TABLE 3
Phantom C: Average CT Attenuation (HU) and PET Activity (kBq/mL) and SD in 4 ROIs: ROI_b and ROI_bt in Phantom Background Inside and Outside CT FOV, Respectively, and ROI_l1 and ROI_l2 in Hot Spheres Inside and on Edge of CT FOV

Image	Phantom position	ROI_b (HU)	*t* test (*P* value)	ROI_bt (HU)	*t* test (*P* value)	ROI_l1 (HU)	ROI_l2 (HU)
CT	Center	−1 ± 16	NA	0 ± 15	0.05	3 ± 10	1 ± 11
	offset_trunc	9 ± 22	<0.001	—	NA	100 ± 200	−500 ± 600
	offset_ext	−15 ± 10	<0.001	−100 ± 20	<0.001	70 ± 200	−10 ± 150
		(kBq/mL)		(kBq/mL)		(kBq/mL)	(kBq/mL)
PET	Center	5.8 ± 0.1	NA	6.0 ± 0.3	<0.001	37 ± 10	43 ± 15
	offset_trunc	5.8 ± 0.2	3 (NS)	0.6 ± 0.2	<0.001	20 ± 5	8 ± 7
	offset_ext	5.7 ± 0.2	0.02	6 ± 1	3 (NS)	31 ± 10	36 ± 12

For location of ROIs, see Figure 1C. *P* values were calculated for CT and PET values independently. We used 2-tailed, paired Student *t* test with Bonferroni correction. Significances were calculated for background only in reference to nontruncated ROI_b.

NA = not applicable; NS = not statistically significant.

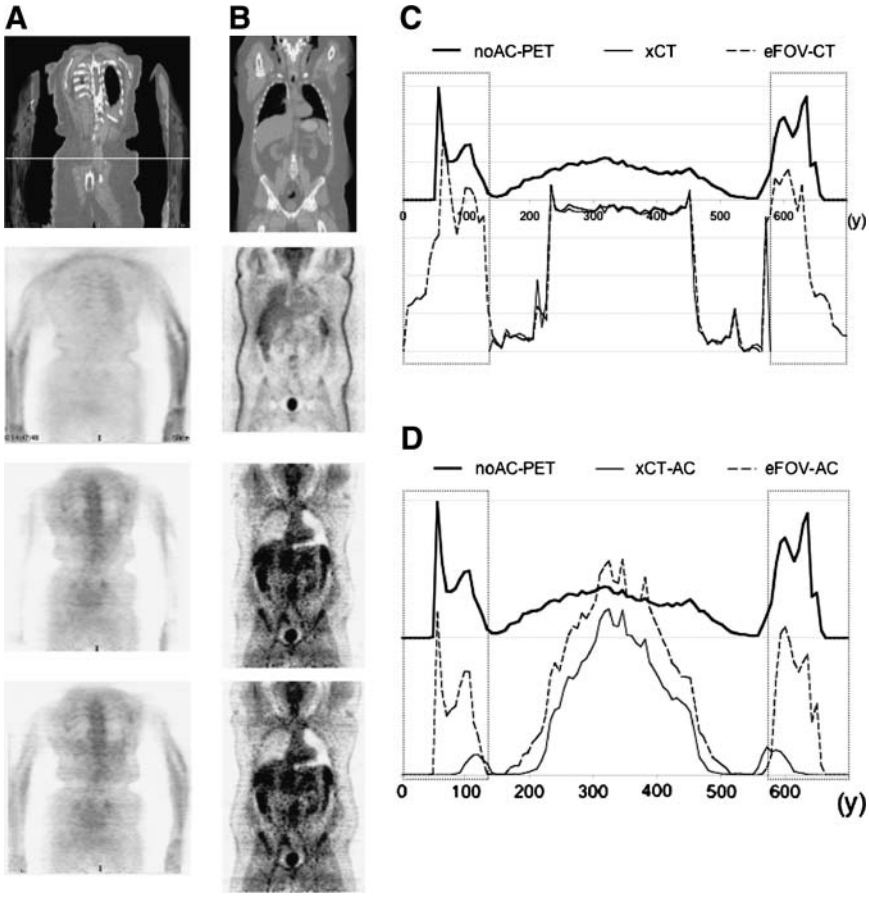

FIGURE 6. Effect of truncation and eFOV correction on patient data from PET/CT using 2-slice (A) and 16-slice (B) CT. Coronal views of fused CT–CT images with truncation and with eFOV recovery (first row), nonattenuation-corrected PET (second row), attenuation-corrected PET with truncated CT (third row), and attenuation-corrected PET with eFOV CT (fourth row). Lateral profiles through CT and PET images of PET/CT study in (A) are shown in (C) and (D), respectively. Boxes on either side of profiles mark the area of truncation. In (D) a relative offset has been added to the profile through the uncorrected PET for improved visibility. noAC PET = PET before AC; xCT = truncated CT, eFOV CT = CT after eFOV correction; xCT AC = PET with AC based on xCT; eFOV AC = PET with AC based on eFOV CT.

studies indicate an underestimation of the attenuation-corrected PET activity of up to 90% in the area of truncation.

Underestimation of tracer activity from truncated CT attenuation maps can be corrected by means of an algorithm (eFOV) proposed originally by Ohnesorge et al. in an attempt to recover object attenuation inside the FOV of clinical CT tomographs (*9*). We have applied this algorithm to the CT data of phantom and patient studies from PET/CT examinations and have further used the extended CT images for a potentially improved AC of the PET data. We found that PET tracer concentrations in the truncated regions can be recovered to at least 84% of the standard activity levels in phantom studies when using CT images after the eFOV correction. In the areas further away from the edge of the CT FOV, the bias from using the truncated CT data for AC can also be reduced through the use of the extended CT images.

In addition to the expected object truncation, we also observed a small but clinically insignificant change of the CT attenuation values inside the CT FOV when scanning the phantoms in the offset position. The corresponding PET activity values in the center of the phantoms (A–C) were not affected by CT truncation (Tables 1–3). This observation supports the fact that local changes on an attenuation map do not necessarily lead to corresponding changes on attenuation-corrected emission images. Instead, the recovery of a local activity distribution is affected by distant artifacts in the attenuation images (such as truncation) as long the AC factors (ACFs) used are computed along the lines of response intersecting these artifacts. Our observation of the central activity values in the attenuation-corrected PET images from the offset_trunc position not being different from those in the center position can be explained by the relatively small number of lines of response (LORs) traversing the area of truncation. The activity concentration in the central portion of the left arm (ROI_ac) in phantom B (Fig. 1B), however, is an exception. Here the relative number of LORs traversing the truncated region of the left arm is much larger and, in addition, beam-hardening effects contribute to an increased variation of CT attenuation values, which propagate into the AC factors and lead to a decrease in the reconstructed PET activity of the central, left arm (Table 2).

When extending the truncated CT projections, as described (*9*), most of the CT object in the vicinity of the CT FOV was recovered, resulting in an average CT attenuation between –100 and –150 HU in the area of truncation in all 3 phantoms. The remaining difference to the attenuation of water (0 HU) is to be expected from the methodology of our implemented eFOV algorithm (*9*) that does not use consistency criteria for full object recovery. Similarly, the eFOV correction algorithm tested here

introduces a slight smearing of the object distribution on CT further away from the maximum CT FOV.

Phantom study C illustrates an important point compared with the uniform phantoms A and B. The uptake in a lesion that is located inside and close to the limit of the measured CT FOV may be obscured by significant CT truncation in the same image plane. Although in our setup neither the lesion inside nor the lesion at the edge of CT FOV was missed when AC was based on the truncated CT data, CT truncation reduced the quantitative lesion recovery to 50% and less. After the eFOV correction, lesion activity concentration increased from 20 kBq/mL (L1) and 8 kBq/mL (L2) to 31 and 36 kBq/mL, respectively, compared with 37 and 43 kBq/mL, respectively, in the center position. It should be pointed out that the activity concentrations in lesions L1 and L2 are prone to partial-volume effects. Given the diameter of L1 (17 mm) and L2 (22 mm) and a spatial resolution of 6–7 mm for the PET system used in our study, we expect an underestimation of the true tracer activity concentration (52.2 kBq/mL) by a factor of 0.7 and 0.8, respectively (Table 3: ROI_l1 and ROI_l2). The remaining difference in the activity concentration in both lesions between the center position and after the eFOV correction is about 11% and can be explained by the rather large fluctuations of the CT attenuation values (ROI_l1, 70 ± 200 HU; ROI_l2, -10 ± 150 HU) after the eFOV correction (Table 3; Fig. 5C).

Thus, phantom C illustrates the importance of correcting for CT truncation artifacts. Especially in follow-up situations with either the pre- or posttherapy PET/CT examination with unaccounted CT truncation, therapeutic response could be assessed wrongly when applying standard therapy response criteria. It is therefore important to consider extended CT attenuation maps for the purpose of more accurate AC and, subsequently, quantitative assessment of the PET tracer uptake as demonstrated in our study. Though careful patient positioning helps avoid truncation artifacts prospectively, in some patients, such as those referred for radiotherapy planning, PET/CT truncation may not be avoided, thus mandating retrospective artifact correction methods. Of course, in either imaging situation, the reader should be encouraged to review the fused PET and CT images carefully, also at the edge of the FOV, to recognize potential image artifacts. The additional consideration of the uncorrected emission images may become useful in cases when artifactual image distortions need to be distinguished from physiologic tracer accumulation but no quantification is needed.

In our study the eFOV correction was applied successfully to a series of patient studies with localized truncation artifacts. Because of lack of a true quantitative verification, we compared the outline of the attenuation-corrected PET images with that of the uncorrected PET images. Since this visual assessment is challenged by the generally poor quality of the low-count images in the case of truncation effects (due to large patients), the advantages of image detruncation in clinical studies cannot always be seen. Therefore, we chose the lateral profiles through the CT and corrected PET data as an alternative quality measure of the efficacy of the eFOV correction and subsequent CT AC.

Despite the excellent recovery of the CT attenuation values inside the patient (Fig. 6C), we noticed a difference in the recovered tracer concentration inside the CT FOV (Fig. 6D), which was somewhat $<30\%$. In part, this difference may be caused by the changes in the CT attenuation whereby the eFOV algorithm recovered a relatively large fraction of the patient anatomy (arms) along the lateral projection (Fig. 6C). Through the calculation of the ACFs for LORs traversing the recovered arm regions, the local recovery of the CT attenuation translates into a significant increase in emission activity after AC. This is seen from the apparent amplification of the pixel-based activity concentration (line profiles in Fig. 6D). Although smearing effects from the calculation of the ACFs in this singular case may help explain the observed difference in activity profiles, further studies across larger patient groups and for different anatomic regions are required. Independently of the reported quantitative effect of the eFOV correction overall quality of the attenuation-corrected PET images inside the CT FOV appeared unaffected, by the eFOV recovery procedure (Fig. 6A). Therefore, we believe that the eFOV correction algorithm implemented here is adequate in recovering the CT attenuation values and PET tracer concentration within the limits of the uncorrected emission data in routine PET/CT.

The idea of compensating for image truncation, specifically for the purpose of AC of radionuclide images, is not new (e.g., (*13,14*)) and has lead to several correction schemes. More recently, a very promising correction algorithm for CT truncation has become available (*15*), which awaits application in WB PET/CT. By incorporating consistency conditions, this algorithm appears to recover larger portions of the truncated objects both inside and outside of the CT FOV, thus generating attenuation data that allow for a more accurate recovery of the tracer activity without being potentially affected by smearing effects in the vicinity of the CT FOV.

CONCLUSION

Truncation artifacts in WB PET AC are observed when scanning large patients or, on occasion, when scanning patients positioned with their arms above the head. Retrospective correction of CT truncation is feasible in state-of-the-art PET/CT and helps to recover the true activity distribution in the PET emission data. In our study, activities in truncated regions could be recovered up to about 90% of the standard activity. Clinically useful patient images can also be obtained with the eFOV correction approach, although more advanced CT-based correction algorithms are being investigated today, which await clinical testing in PET/CT.

ACKNOWLEDGMENTS

We thank Otto Sembritzki (Siemens CT, Forchheim, Germany) for his assistance with the processing of part of the CT data. We also thank our technologists Coletta Kruschke, Nicole Henke, Brigitte Dzewas, and Jutta Grahneis; Angelika Bildstein, Bärbel Terschüren, Dorothea Porsch-Plottek, and Sandra Pabst, and Slavko Maric for their assistance and cooperation during these studies.

REFERENCES

1. Czernin J, Schelbert H. PET/CT imaging: facts, opinions, and questions. *J Nucl Med.* 2004;45(suppl 1):1S–3S.
2. Beyer T, Townsend DW, Brun T, et al. A combined PET/CT tomograph for clinical oncology. *J Nucl Med.* 2000;41:1369–1379.
3. Kinahan PE, Hasegawa BH, Beyer T. X-ray-based attenuation correction for positron emission tomography/computed tomography scanners. *Semin Nucl Med.* 2003;33:166–179.
4. Burger C, Goerres G, Schoenes S, Buck A, Lonn AHR, von Schulthess GK. PET attenuation coefficients from CT images: experimental evaluation of the transformation of CT into PET 511-keV attenuation coefficients. *Eur J Nucl Med Imaging.* 2002;29:922–927.
5. Beyer T, Townsend DW. Dual-modality PET/CT acquisition systems for clinical oncology. In: Oehr P, Biersack H-J, Coleman E, eds. *PET and PET/CT in Clinical Oncology.* Heidelberg, Germany: Springer; 2003:9-28.
6. National Electrical Manufacturers Association. *Performance Measurements of Positron Emission Tomographs: NEMA Standards Publication NU 2-2001.* Rosslyn, VA: NEMA; 2001.
7. Kinahan PE, Townsend DW, Beyer T, Sashin D. Attenuation correction for a combined 3D PET/CT scanner. *Med Phys.* 1998;25:2046–2053.
8. Schaller S, Semrbitzki O, Beyer T, Fuchs T, Kachelriess M, Flohr T. An algorithm for virtual extension of the CT field of measurement for application in combined PET/CT scanners [abstract]. *Radiology.* 2002;225(P):497.
9. Ohnesorge B, Flohr T, Schwarz K, Heiken JP, Bae KT. Efficient correction for CT image artifacts caused by objects extending oustide the scan field-of-view. *Med Phys.* 2000;27:39–46.
10. Beyer T, Antoch G, Blodgett T, Freudenberg L, Akhurst T, Mueller S. Dual-modality PET/CT imaging: the effect of respiratory motion on combined image quality in clinical oncology. *Eur J Nucl Med Imaging.* 2003;30: 588–596.
11. Antoch G, Kuehl H, Kanja J, et al. Dual-modality PET/CT scanning with negative oral contrast agent to avoid artifacts: introduction and evaluation. *Radiology.* 2004;230:879–885.
12. Beyer T, Antoch G, Bockisch A, Stattaus J. Optimized IV contrast administration protocols for diagnostic PET/CT imaging. *J Nucl Med.* 2005;46:429–435.
13. Manglos S. Truncation artifact suppression in cone-beam radionuclide-transmission CT using maximum likelihood techniques: evaluation with human subjects. *Phys Med Biol.* 1992;37:549–562.
14. Kadrmas DJ, Jaszczak RJ, Cormick JM, Coleman RE, Lim CB. Truncation artifact reduction in transmission CT for improved SPECT attenuation correction. *Phys Med Biol.* 1995;40:1085–1104.
15. Sourbelle K, Kachelriess M, Kalender WA. Reconstrcution from truncated projections in CT using adaptive detruncation. *Eur Radiol.* 2005;15:1008–1014.